Polymer 58 (2015) 170–179

Contents lists available at ScienceDirect

Polymer

journal homepage: www.elsevier.com/locate/polymer

Visualization of micro-scale inhomogeneities in acrylic thickener solutions: A multiple particle tracking study

A. Kowalczyk, C. Oelschlaeger*, N. Willenbacher

Karlsruhe Institute of Technology (KIT), Institute of Mechanical Process Engineering and Mechanics, Gotthard-Franz-Str.3, 76128 Karlsruhe, Germany

ARTICLE INFO

Article history:
Received 1 September 2014
Received in revised form
17 November 2014
Accepted 20 December 2014
Available online 27 December 2014

Keywords:
Microrheology
Multiple particle tracking (MPT)
Heterogeneous fluids

ABSTRACT

Multiple Particle Tracking (MPT) microrheology in combination with bulk mechanical rheometry has been used to characterize the structural and viscoelastic microheterogeneity of commercial acrylic thickeners Carbopol EDT2050, Viscalex HV30, and Sterocoll D in aqueous solutions at technically relevant polymer concentrations. According to bulk rheology Carbopol solutions exhibit a much higher elasticity than Sterocoll and Viscalex solutions at low polymer concentration whereas all thickeners are composed of similar main monomers. MPT experiments confirm that the latter two systems form homogeneous predominately elastic polymer networks with a mesh size <200 nm. In contrast, Carbopol solutions are highly heterogeneous and the degree of heterogeneity strongly increases with increasing polymer concentration. Predominantly elastic and viscous regions within the solution can be identified based on the slope of the mean squared displacement of individual particle trajectories. This heterogeneity is directly imaged here for the first time using Voronoi diagrams and characteristic length scales varying from 5 to 20 μm are found. Additionally, variation of the probe size reveals that the elastic regions themselves are heterogeneous including areas with mesh size <200 nm and a larger fraction with mesh size between 200 nm and 500 nm.

1. Introduction

Synthetic acrylic polymers are frequently used as thickening agents in water-based coatings and adhesives or personal care products. Typically, these commercial alkali-swellable acrylates [1–4] (as well as various other polymeric thickeners) form inhomogeneous partly aggregated or cross-linked solutions. Inter- and/or intramolecular aggregation is due to hydrophobic groups randomly distributed along the chains and the swelling behavior can be varied via solvent quality [5–7]. Crosslinking can be induced either thermally or by adding appropriate crosslinking agents during synthesis. Accordingly, such thickener solutions cover a wide range of rheological behavior, ranging from weakly elastic, almost Newtonian to highly elastic gel-like. Despite its high technical relevance, little is known so far about the contribution of the micro-scale inhomogeneity to the bulk viscoelastic properties [8]. Here we use the method of Multiple Particle Tracking (MPT) to quantify the degree of structural and mechanical microheterogeneity of such acrylic thickener solutions. This technique was originally described by Apgar et al. [9] and Ma et al. [10]. Up to now MPT has been frequently used to study microheterogeneities of actin filament network [11–14], living cells [15–19], proteins [20,21], DNA solutions [22], biological gels [23,24] or yield stress fluids [1–3]. The fluid mechanics of microrheology has been described thoroughly [25,26]. The basic idea is to monitor the Brownian motion of inert fluorescent tracer particles by means of digital video microscopy. For homogeneous fluids the bulk shear moduli [27] can be determined using this technique, but more importantly the statistical analysis of tracer trajectories allows for a characterization of sample inhomogeneity. Al least some hundred particles have to be monitored simultaneously to allow for a significant statistical analysis in order to cover a sufficiently large area of the samples. For a better interpretation and characterization of the heterogeneous dynamics and/or microstructure, statistical distributions of displacement and local viscosity [11,22,23,28,29] but also van Hove correlation plots and the non-Gaussian parameter α [30–33] are used to characterize the heterogeneous and microstructure of fluids. The non-Gaussian part of the van Hove correlation function $G_s(x,\tau)$ [32,33] is defined as the probability density distribution of the displacements of individual particles [32,34]:

* Corresponding author.
E-mail address: claude.oelschlaeger@kit.edu (C. Oelschlaeger).

http://dx.doi.org/10.1016/j.polymer.2014.12.041
0032-3861/

$$G_s(x,\tau) = \frac{1}{N}\langle \sum_{i=1}^{N} \delta[x + x_i(0) - x_i(\tau)]\rangle = \frac{N(x,\tau)}{N} \quad (1)$$

with X the distance of particle center of mass along the X -coordinate. N(X,τ) is the number of particles found at positions between X and (X + d X) after lag time τ and N is the total number of particles. If all particles are exposed to similar environment $G_s(x,\tau)$ has a Gaussian form. Deviations from this form reflect the presence of heterogeneities. Such deviations can be characterized by the non-Gaussian parameter

$$\alpha = \frac{\langle x^4(\tau)\rangle}{3x^2(\tau)^2} - 1 \quad (2)$$

with $\langle x^b(\tau)\rangle = \sum_{i=1}^{N} x_i^b(\tau) * G_s(x,\tau)$ the simplest combination of the second (b = 2) and fourth (b = 4) moments of a one-dimensional probability density function. α is zero for a Gaussian distribution, while distributions result in large values of α [30,33].

In the first part of the paper, we characterize bulk rheological properties of the three different acrylic thickeners and investigate variations of yield stress σ_y and plateau modulus G_0 as a function of polymer concentration. In the second part, we describe and use the MPT method to perform microrheological measurements on thickener solutions presenting similar bulk elastic properties, i.e. similar G_0 values. For those samples, we generate the variation of mean square displacements (MSD) as a function of time and from statistical analysis of the MSD distribution we extract microstructural and micro-mechanical heterogeneity informations. Additionally, for Carbopol only we investigate probe size and polymer concentration effects on microrheological properties in order to get additional microstructural information. Finally, we use Voronoi diagrams constructed using the particle positions as generators in order to visualize the size and spatial distribution of heterogeneities based on a "rheological contrast", i.e. classification of particle mobility and hence viscoelasticity of its surrounding according to the slope of the respective MSD.

2. Materials and methods

2.1. Samples

Our experiments were performed using three acrylic thickeners, Sterocoll D, Viscalex HV 30 (both from BASF SE Ludwigshafen, Germany) and Carbopol ETD 2050 (Lubrizol Advanced Materials, Cleveland, USA). For brevity, we use the family name of each product in the subsequent text. These are commercial, alkali-swellable thickeners based on homopolymers and co-polymers of polyacrylic acid and a small amount of a crosslinking agent [7,35]. Upon neutralization the weak acrylic acid groups dissociate in aqueous environment, the polymer chains get soluble and the thickening properties are developed. Sterocoll is mainly used as rheology modifier for rotogravure and paper coating [36] and Viscalex for water-borne coating [37,38]. Both are synthesized in an emulsion polymerization process and delivered as a milky liquid with a solids content of 25%–30% and pH ≈ 2.5–3. In both cases, main monomers are ethylacrylate (EA) and methacrylic acid (MAA). Sterocoll is an alkali swellable emulsion polymer (ASE) with a MAA/EA molar ratio of about 50:50 and a small fraction of diethylenically unsaturated monomer as chemical crosslinker. Viscalex differs in a sense that it is a hydrophobically modified alkali swellable emulsion (HASE). It contains hydrophobic alkyl groups attached to its polymer backbone. The molar ratio MAA/EA/Alkyl is about 49:50:1. In aqueous solution, hydrophobic association junctions are formed providing side chains physical crosslinking. Structure representations for these types of polymers are shown in studies of Ng et al. [6], Dai et al. [39] and Wang et al. [5]. For the investigations presented here, aqueous solutions of Sterocoll with concentrations of 0.25–5wt. % and Viscalex with concentrations of 0.25–1.5 wt.% were prepared. Solutions were stirred at room temperature for 48 h and adjusted to pH = 8 by slowly adding 1 N NaOH [4,7]. Carbopol ETD 2050 consists of high molecular weight polymers, made up of homopolymers of acrylic acid and copolymers of acrylic acid and long chain (C10–C30) alkyl acrylate crosslinked with a polyalkenyl polyether. Illustration of the Carbopol structure is shown in Ref. [40]. The carboxylic groups are the principle chemical sites that affect the thickening characteristics. It is supplied as powder. We prepared samples (0.1–1wt.%) by slowly adding powder in water, which decreases the pH to 3 while stirring, consequently carboxylic groups release the hydrogen atom. The mixture was further stirred at room temperature for 48 h and adjusted to pH = 6 by slowly adding 4 N NaOH. Neutralization replaces a free hydrogen cation with the sodium cation and the repulsive force between the negatives charges of the carboxyl groups and osmotic pressure from mobile ions cause the structure to swell, resulting in a highly elastic microgel system optically transparent, but known to exhibit an inhomogeneous structure on the micrometer scale [1,2]. Increasing the pH further does not change the viscoelastic elastic properties very much. Carbopol is used in applications including clear gels, hydroalcoholic gels and lotions [41].

2.2. Mechanical measurements

A rotational rheometer Thermo MARS II equipped with a cone-plate measuring cell (diameter $d_{CP} = 60$ mm, cone angle $\alpha_{cone} = 1°$) was used to perform steady as well as small amplitude oscillatory shear experiments. The latter covering the frequency range from 0.01 to 100 rad.s^{-1}. Strain sweep experiments performed prior to frequency sweeps ensure that the strain amplitude used was sufficiently small to provide a linear material response at all investigated frequencies. The yield stress was determined by fitting a Herschel–Bulkley model to the shear rate/shear stress data obtained from stress ramp experiments covering the stress interval from 0.1 Pa to 50 Pa within a measuring time of 1800 s. All measurements were performed at 20 °C and a solvent trap was used to avoid evaporation of the solvent during the experiments.

2.3. Multiple-particle tracking (MPT) setup

MPT experiments were performed using an inverted fluorescence microscope (Axio Observer D1, Zeiss), equipped with a Fluar 100×, N.A. 1.3, oil-immersion lens combined with a 1x optovar magnification changer. We have tracked the Brownian motion of green fluorescent polystyrene microspheres of 0.19, 0.51 μm diameter (Bangs Laboratories: USA, lot Nr FC03F/7049) used as tracer particles. The mixture (total volume: ~20 μl) containing the sample solution including the tracers (volume fraction around 1%) was injected into a commercial rectangle capillary (CM Scientific Ltd, United Kingdom). The sample thickness was ~150 μm and the microscope was focused roughly halfway into the sample to minimize wall effects. Images of the fluorescent beads were recorded onto a personal computer via a sCMOS camera Zyla X (Andor Technology: 21.8 mm diagonal sCMOS Sensor size, 2560 × 2160 square pixels (6.5 μm), up to 50 frames/s in global shutter mode). Displacements of particle centers were monitored in an 84 × 84 μm field of view, for at least 100 s at a rate of 30 frames/s. For each experiment a total of roughly 300 particles were tracked simultaneously. Movies of the fluctuating microspheres were analyzed by a custom MPT routine incorporated into the software Image Processing System (Visiometrics iPS) and a self-written Matlab program [42]. Tracing errors due to particles moving in and out of the

focal plane are a fundamental problem of two dimensional MPT microrheology; these errors have been eliminated using an advanced tracing algorithm called radius of gyration (RG) criterion which is based on the widely used Crocker and Grier tracking algorithm [43]. The particle displacements between subsequent images are identified as so-called artificial jumps if this displacement deviates more than four standard deviations from the mean value and trajectories are terminated at such positions. In the subsequent processing step trajectories which are separated by a time gap not larger than $\Delta\tau_{max}$ are merged based on an adaptive search radius criterion taking into account a reduced radius of gyration and the individual particle mobility. Data analysis relies on a reasonable choice of $\Delta\tau_{max}$ and the accessible time scale depends on a minimum number of time steps or length L_{min} of the trajectories accepted for further analysis. This data processing and analysis scheme is thoroughly described in Ref. [42]. Additionally, a homogenous distribution of the tracer particles embedded in the probe is necessary to allow for a meaningful interpretation of the microstructure of the investigated thickener solutions. This has been evaluated calculating the function g(r) from all particle positions within an image. Corresponding results are shown in Fig. 1 for solutions of all three thickeners types investigated here. In all cases an almost ideal behavior with $g(r) \approx 1$ is found, indicating a homogenous particle distribution in all samples.

3. Results and discussion

3.1. Bulk rheology measurements

Characterization of bulk viscoelastic properties of the three acrylic thickener solutions has already been performed in many rheological studies [1–3,7,42,44–46]. These solutions exhibit a strong gel like behavior and an apparent yield stress. Even at low polymer concentration of 1% we found yield stress values of $\sigma_y = 10.3 \pm 0.6$, 6.0 ± 0.6 and 2.2 ± 0.5 Pa for Carbopol, Viscalex and Sterocoll, respectively. Fig. 2A shows the plateau modulus $G_0 = G'$ ($\omega = 1$ rad.s^{-1}) determined from oscillatory shear measurements as a function of polymer concentration for the three thickeners.

An important observation is that at low polymer concentration G_0 is much higher for Carbopol (squares) than for Viscalex (triangles) and Sterocoll D (circles) solutions, e.g. a concentration of 0.25% $G_0 \sim 25$ Pa for Carbopol whereas it is only 1 and 0.05 Pa for Viscalex and Sterocoll, respectively. This strong difference is intriguing especially from a technical point of view as the three thickeners comprise with similar main monomers. Another difference resides in the concentration dependence of G_0. For Carbopol this variation is described by a simple power-law dependance $G_0 \sim c^{3/4}$ linear over the full concentration range investigated. The moduli of Viscalex and Sterocoll exhibit a much stronger concentration dependence especially at concentration below 1% but start at much lower values. In order to gain a better understanding of these bulk rheological differences, we have investigated the microrheological properties of three thickener solutions with similar bulk elastic properties; i.e. similar plateau modulus G_0, using MPT. Solutions of 0.3% Carbopol, 0.5% Viscalex and 2% Sterocoll exhibit G_0 values between 21 and 29 Pa considered to be equal within experimental error (see hatched box in Fig. 2A). As can be seen from Fig. 2B the variation of dynamic shear moduli G′ and G″ with frequency is almost similar in the whole frequency range investigated ($0.01 < \omega < 100$ rad.s^{-1}). The storage modulus G′ is always larger than the loss modulus G″ (G′ G″) and no crossover is observed indicating a very long terminal relaxation time (>100 s). Nevertheless, we observe a weak G′ increase as a function of ω for Sterocoll and Viscalex solutions. The latter result may be explained by higher molecular weight polydispersity compared to Carbopol. Chains of different length whose stress contributions will relax at different rates lead to this slight G′ dependence. Additionally, by extrapolating G′ and G″ at low frequencies, we can predict a G′, G″ crossover that will occur at a certain frequency ω_c for both Sterocoll and Viscalex solutions indicating a terminal flow regime. Terminal shear relaxation times for Sterocoll and Viscalex solutions have been reported in Martinie et al. [47] and Kowalczyk et al. [48]. For both samples, at the polymer concentrations investigated here, relaxation times of about $T_R = 1/\omega_c \sim 900$ s were found. For Carbopol solutions, no relaxation time data are found in the literature but according to Fig. 2B, T_R must be much larger than for the Sterocoll or Viscalex solutions investigated here if it exists at all. It seems that the heterogeneous structure with its sample-spanning network of highly elastic regions hinders or at least delays stress relaxation compared to the homogeneous Viscalex and Sterocoll solutions. Finally, we can directly determine the mesh size ξ of the polymer network from the plateau modulus value G_0. According to the classical theory of rubber elasticity $G_0 = k_BT/\xi^3$ [49] and $G_0 = 25$ Pa corresponds to $\xi = 55$ nm. This value is much smaller than the diameter of the embedded tracer particles (~500 nm) used for MPT measurements. Therefore, we can treat the medium as a continuum around the embedded probe particles.

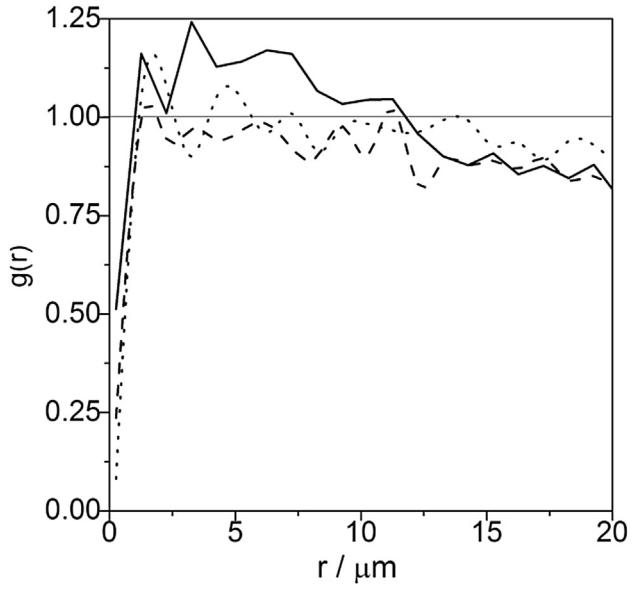

Fig. 1. Pair correlation function g(r) as a function of distance r for Viscalex 0.5% (dashed line), Sterocoll 2% (dotted line) and Carbopol 0.3% (full line) solutions.

3.2. Microrheology measurements

As mentioned previously, microrheological measurements have been performed on samples showing similar bulk elastic properties. Fluorescent polystyrene microspheres ~500 nm in diameter have been used as tracer particles. Particle trajectories were constructed using the track algorithm in combination with the RG criterion described in Section 2C. The corresponding MSD traces for Carbopol, Sterocoll and Viscalex are shown in Fig. 3A-C, respectively.

For Carbopol (Fig. 3A), the range of displacement at a given lag time is very broad, e.g. $\tau = 1/10$ s, MSD varies more than two orders of magnitude, from 7.10^{-5} to 8.10^{-3} μm^2. The lowest MSD value of 7.10^{-5} μm^2 obtained at the shortest lag time $\tau = 1/30$ s exceeds the resolution of our setup which is about 3.10^{-5} μm^2 thus the so called static error correction as described in Ref. [50] can be neglected. A substantial fraction of MSD traces adopt a power-law behavior as a

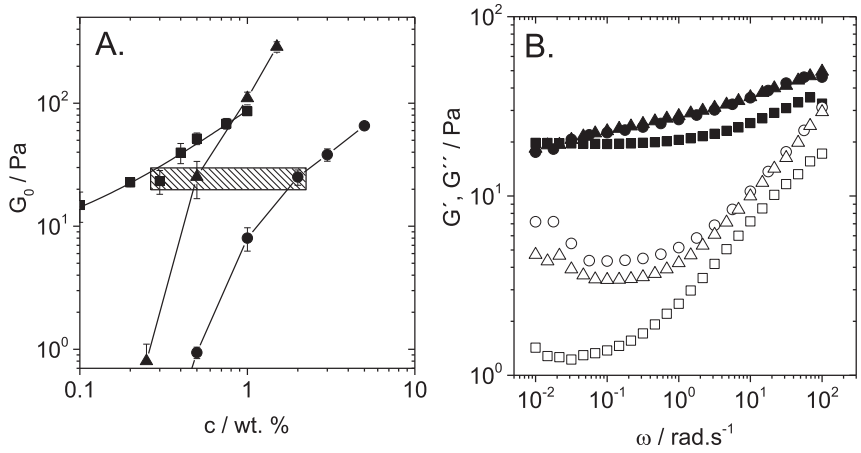

Fig. 2. A) Plateau modulus G_0 as a function of acrylic thickener concentration. Hatched box highlights the three samples investigated with MPT. B) Frequency dependence of shear moduli G′ (closed symbols) and G″ (open symbols) for Sterocoll 2% (circles), Viscalex 0.5% (triangles) and Carbopol 0.3% (squares).

function of time $\langle \Delta r^2(\tau) \rangle \propto \tau^{\beta}$ with a slope β close to 1 throughout the probed time scales. This result indicates that the motion of these beads is purely diffusive and that the microenvironment surrounding the particles responds like a viscous liquid. Other MSD traces exhibit a curvature and the power law exponent tends towards $\beta = 0$ at long lag times indicating that the particles are highly constrained by the surrounding solution. In that case, the motion is subdiffusive which is the signature of elastic trapping of the beads in the solution. This result clearly reveals a strong heterogeneity of the Carbopol solution on the μm length scale as already reported by Oppong et al. [2,3] who suggest that the microstructure of Carbopol gels consists of concentrated centers of strongly cross-linked polymer molecules surrounded by regions of more dilute polymer. Roberts et al. [44] proposed the structure of an existing highly-crosslinked core with overlapping dangling ends in a viscous environment. Another structure has been suggested by Kim et al. [46] based on cryo-scanning electron microscopy (cryo-SEM). These images suggest a transition from a string-like entangled structure to a honeycomb-like rigid structure (pore size ~5 μm) with increasing polymer concentration.

In Sterocoll solution (Fig. 3B) microspheres move significantly different. Here almost all MSDs depend only weakly on time (β ~0.1) for τ < 10s, indicating that particles are highly constrained by the surrounding solution. This result is consistent with an elastic trapping of tracer particles in a homogeneous gel-like environment. At long times (τ > 10 s) the slope of the MSD traces approaches $\beta = 1$ indicating slow viscous diffusion of the beads corresponding to a transition into the terminal flow regime. Compared to the Carbopol solution, the range of displacements at a given time is much narrower; it varies e.g. from 3.10^{-4} to 2.10^{-3} μm² at τ = 0.1 s. Similar behavior is observed for the Viscalex solution (Fig. 3C). In this case MSD traces exhibit a plateau throughout all the probed time scales, no MSD increase is observed at long lag times indicating a longer relaxation time τ_R > 30s. Moreover, similar MSD variations have been obtained for Sterocoll and Viscalex solutions using tracer particles with diameter 200 nm. This result indicates that the mesh size of the polymer network in both systems is clearly below 200 nm which is in good agreement with the mesh size value ξ_{bulk} = 55 nm determined from bulk G_0 data based on classical rubber elasticity theory. In summary, MPT measurements show that Carbopol is strongly inhomogeneous on the μm-scale whereas Sterocoll and Viscalex are both homogeneous solutions at the polymer concentrations investigated here.

3.2.1. *Van Hove correlation function*

In Fig. 4 we report the van Hove correlation functions in order to perform the statistical analysis of the distribution of displacements for Carbopol 0.3%, Sterocoll 2% and Viscalex 0.5% solutions calculated at a lag time τ = 3s. This lag time value has been chosen arbitrarily as the non-Gaussian parameter α extracted from this analysis is almost independent of time (result not shown). For the Viscalex solution (blue cross) we observe that the MSD data are

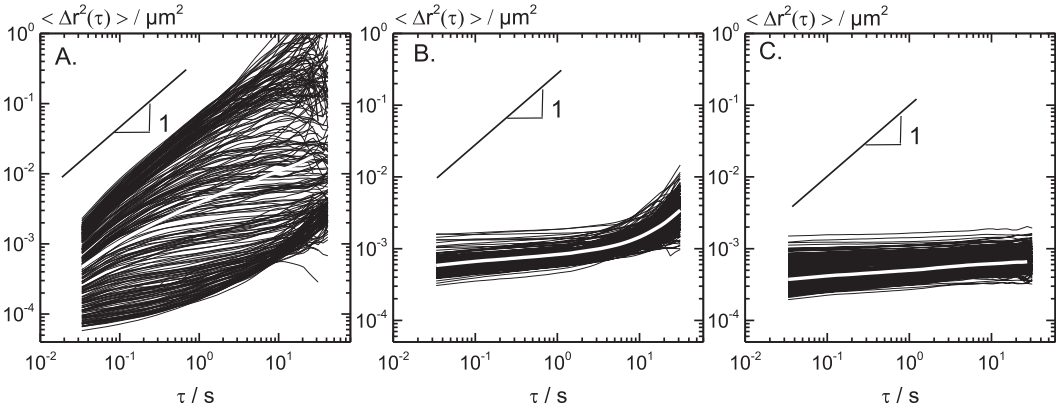

Fig. 3. Mean square displacement of microspheres (~500 nm) dispersed in aqueous solution of Carbopol 0.3% (A), Sterocoll 2% (B) and Viscalex 0.5% (C). The white curve is the ensemble-average MSD.

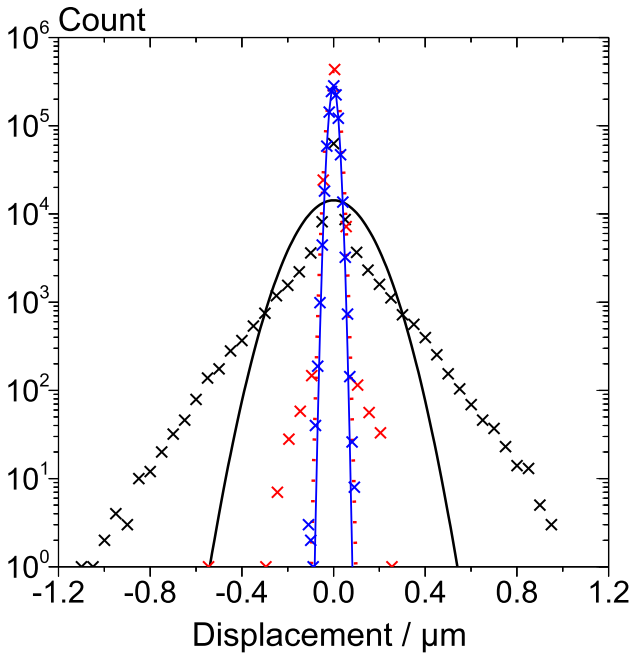

Fig. 4. Van Hove correlation functions for the ensemble particles at time lag $\tau = 3$s for Carbopol (black), Sterocoll (red), Viscalex (blue). The lines show the Gaussian fit to the data.

described by a Gaussian distribution obtained at a given lag time indicating that all tracer particles exhibit similar diffusivity. The low value of $\alpha = 0.15$ is a strong indicator of a homogeneous system. For Sterocoll (red cross) we find $\alpha = 0.4$. Although this value is slightly higher than that obtained for the Viscalex solution, it still confirms a high degree of homogeneity of the system. Finally, for the Carbopol solution (black cross) we observe a strong deviation of the measured displacements from a Gaussian distribution with $\alpha = 4$. This again clearly manifests the high degree of heterogeneity compared to the other two solutions.

Table 1 shows the variation of α for all three solutions as a function of polymer concentration.

For Sterocoll and Viscalex solutions α is independent of polymer concentration within experimental error. In both cases α values are less than one (~0.5) indicating homogeneous systems independent of polymer concentration. On the contrary, for the Carbopol solution α increases from ~1.5 to ~7 when the polymer concentration increases from 0.1 to 0.75%, respectively. This strong increase in α indicates that the Carbopol micro-structure becomes more and more heterogeneous as the polymer concentration increases. This will be discussed in more detail in the next section.

3.2.2. MSD distributions and statistical analysis

To quantify the level of inhomogeneity in the different solutions we generate the MSD slope dMSD/dτ distributions (Fig. 5) and MSD distributions (Fig. 6) calculated from the individual microspheres trajectories at a lag time $\tau = 3$s. For both Sterocoll (Fig. 5B) and Viscalex (Fig. 5C) solutions, the MSD slope distribution is narrow with almost all values <0.5 and <0.3, respectively indicating a homogeneous strongly elastic environment. On the contrary, for the Carbopol solution (Fig. 5A) the distribution of the dMSD/dα values is very broad and asymmetric with approximately 70% of MSD data having a slope <0.5, indicating a more elastic environment and 30% > 0.5 corresponding a more viscous surrounding.

This result is confirmed by the distribution of absolute MSD values obtained at a lag time $\tau = 3$s shown in Fig. 6A–C.

For the Carbopol solution (Fig. 6A) the MSD distribution is bimodal with a majority of particles having MSD absolute values around 10^{-2} μm^2 and a second population with a broad distribution of MSDs centered around 10^{-1} μm^2. For Sterocoll (Fig. 6B) and Viscalex (Fig. 6C) solutions, the distribution is narrow and in both cases all MSD absolute values are well below 10^{-2} μm^2.

Fig. 7A–C characterize the micro-structure of the solutions by plotting all particles positions in the plane of observation; color coding each individual position according to the MSD slope assigning a circular area for each data point corresponding to the MSD of the respective particle. This representation allows us to physically map the variation in the local mechanical response across the sample and to directly get information about the distribution of elastic and viscous regions throughout the sample. It should be noted that this representation is different from that introduced by Valentine et al. [13] where in their study trajectories are color coded according to cluster analysis. They define a cluster as a group of particles where all the particles in a given cluster are statistically indistinguishable. In a first approach, we clearly see that the displacement of embedded beads in a Carbopol solution (Fig. 7A) is completely different from that observed in Sterocoll (Fig. 7B) and Viscalex (Fig. 7C) solutions. For the two latter solutions, almost all particles show a small dot size and a similar color code (red). This representation again confirms that both samples are highly homogeneous elastic materials on the length scale of the probe particles (~500 nm). On the contrary, the map indicates a strong heterogeneity of the Carbopol solution in terms of color code and dot size characterizing the mobility of the individual particles. In this case, the sample is inhomogeneous on the μm length scale with particles that move freely within viscous region of about 10 μm in size surrounded by elastic areas where tracer mobility is highly restricted.

3.2.3. Variation of polymer concentration

In this section, we discuss the effect of polymer concentration on microrheological properties in order to obtain additional information about the structure. Fig. 8 shows the variation of the scaling exponent β of the ensemble-average MSD ~ τ^β as a function of Sterocoll and Viscalex concentration.

For Sterocoll, β decreases continuously from about one to zero when increasing the polymer concentration from 0.25 to 3%. At the same time, the values for the non-Gaussian parameter α are found to be less than one independent of Sterocoll concentration within experimental error (see Table 1). This result indicates a transition from a homogeneous Newtonian fluid to a homogeneous highly elastic gel-like material. A uniform network forms with gradually decreasing mesh-size as polymer concentration increases. Similar results have been obtained for Viscalex solutions, i.e. the non-Gaussian parameter (α~0.2) is independent of Viscalex concentration, but β decreases monotonically with polymer concentration, again indicating a uniform homogeneous network structure. In both systems, the tracer particles used (diameter 500 nm) are much larger than the mesh size of the polymer network. A different completely behavior is obtained for the Carbopol solutions when varying the polymer concentration. At 0.1% concentration (Fig. 9A), the MSD slope distribution shows a majority of particles (~85%)

Table 1
Non-Gaussian parameter α for all three thickeners in solutions with different polymer concentration.

Carbopol wt%	α	Sterocoll wt%	α	Viscalex wt%	α
0.1%	1.6 ± 0.26	0.25%	0.2 ± 0.06	0.5%	0.15 ± 0.09
0.3%	3.5 ± 0.65	0.5%	0.35 ± 0.13	1%	0.15 ± 0.10
0.75%	6.8 ± 0.86	2%	0.4 ± 0.08	1.5%	0.39 ± 0.09

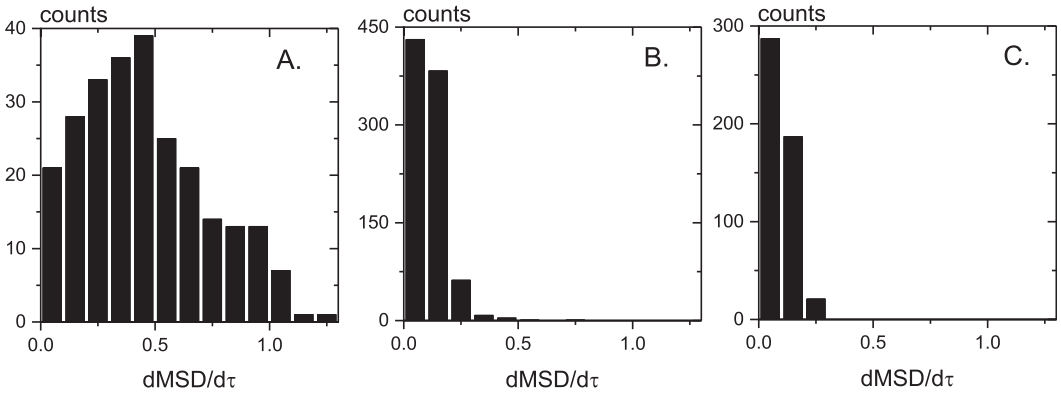

Fig. 5. Distributions of MSD slopes measured at time lag $\tau = 3s$ 3s for microspheres (0.5 μm) dispersed in an aqueous solution of Carbopol 0.3% (A), Sterocoll 2% (B) and Viscalex 0.5% (C).

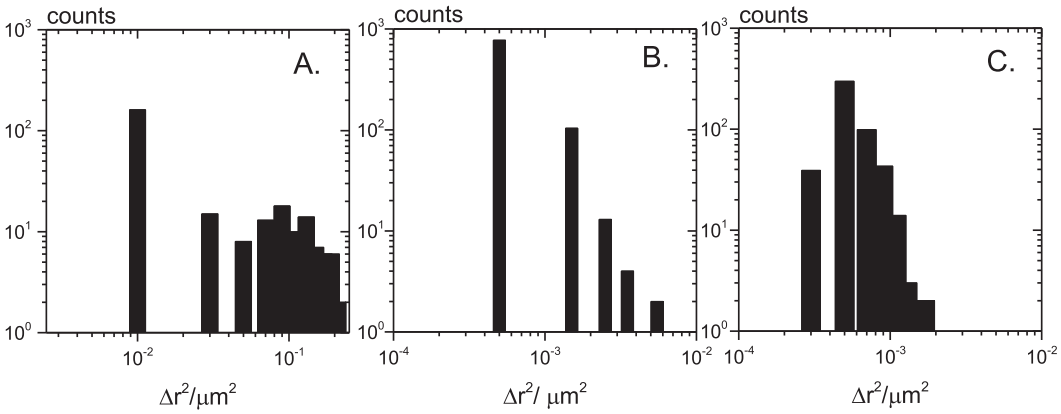

Fig. 6. MSD distributions measured at time lag of $\tau = 3s$ for microspheres (0.5 μm) dispersed in an aqueous solution of Carbopol 0.3% (A), Sterocoll 2% (B) and Viscalex 0.5% (C).

with slopes >0.5 and a peak around 0.75, indicating that almost all particles see a predominantely viscous environment. At a concentration of 0.3% (Fig. 9B), the solution becomes heterogeneous with ~65% of particles being in an elastic environment (dMSD/dα <0.5) and ~35% moving freely (see comments of Fig. 5A). Finally at a concentration of 0.75% (Fig. 9C), only ~15% of particles move freely and a majority (~85%) is confined in a strongly elastic environment.

Strong heterogeneities of such Carbopol solutions and a similar variation of dMSD/dα distributions as a function of polymer concentration have been observed by Oppong et al. [3] in their MPT experiments with tracer particles of diameter 1 μm. In their study no probe size variation has been performed. Furthermore small angle light scattering experiments [51] have shown that Carbopol solutions consist of microgel particles with a strongly crosslinked core approximately 500 nm in diameter surrounded by a highly expanded shell of polymer chains ~20 μm in size. This shell has a low monomer concentration as well as a low crosslink and/or entanglement density. The highly crosslinked core of the microgel particles is not accessible for the tracer particles but they can move diffusively through the shell. Accordingly, at low Carbopol

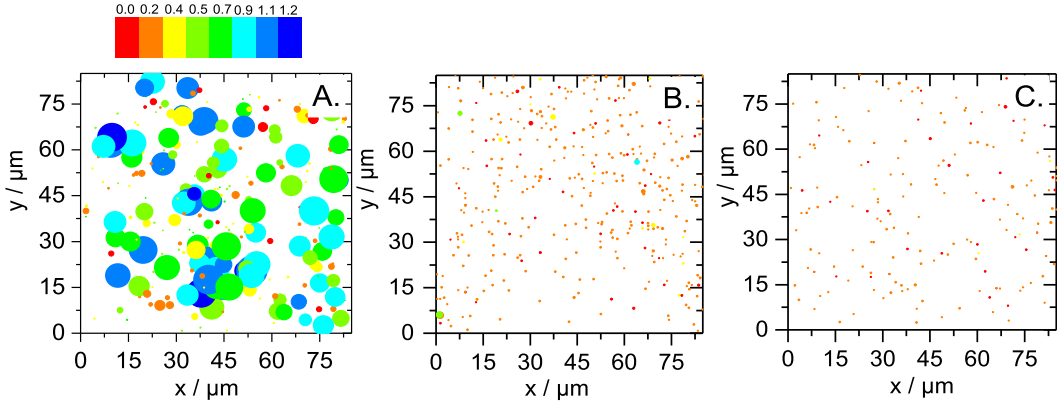

Fig. 7. Visualization of heterogeneity: x, y positions of individual embedded beads, with corresponding mean free path (dot size) multiplied by a factor of 40, and corresponding slope of MSD (color scale) for Carbopol (A), Sterocoll (B) and Viscalex (C).

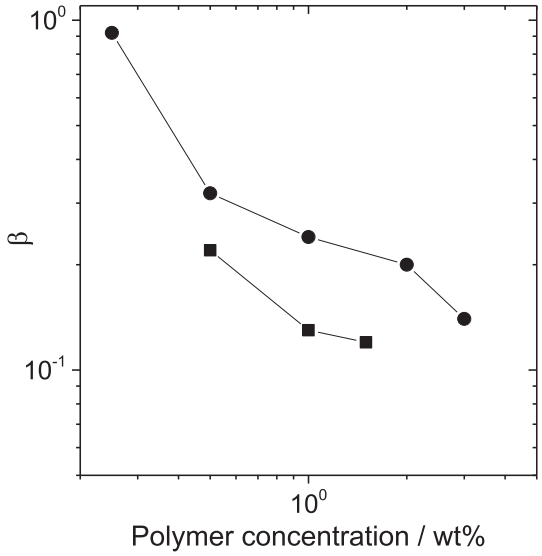

Fig. 8. Variation of the scaling exponent β of the ensemble-average MSD as a function of Sterocoll (circles) and Viscalex (squares) concentrations. Diameter of the tracer particles was 500 nm.

concentrations the solution appears homogeneous, the α-parameter is low and essentially all tracer particles explore a viscous environment (see Fig. 10). As the polymer concentration increases, the microgel particles start to interpenetrate thus forming elastic regions with high entanglement or crosslinks density. These elastic regions grow and the fraction of tracer particles in a viscous environment decreases with increasing polymer concentration. Accordingly, the non-Gaussian parameter characterizing solution heterogeneity increases with increasing polymer concentration as shown in Fig. 10. A schematic sketch of this change in microstructural heterogeneity is provided in Fig. 11. Finally, the fraction of particles in a viscous environment reaches a minimum value of about 0.2 at a polymer concentration of 0.75% and the non-Gaussian parameter levels off at $\alpha \approx 7$.

Further information about the complex microstructure of Carbopol solutions is gained from additional MPT measurements using tracer particle of the same nature but with a lower diameter of 190 nm. Preliminary measurements ensured that these smaller tracer particles were homogeneously distributed by calculating the pair correlation function g(r) which was almost equal to 1 independent of r. We focused on the sample with Carbopol concentration 0.3% and found that approximately ~80% of tracer particles with diameter 190 nm are in a viscous environment compared to 35% for tracers with diameter 520 nm. Corresponding non-Gaussian parameter values are ~0.5 and ~4, respectively. The fact that the majority of particles with diameter 190 nm moves freely indicates that the mesh size in most of the elastic, entangled regions is greater than 200 nm. This further elucidates the heterogeneity of the solution consisting of few regions with a mesh size smaller than 200 nm and a major fraction of areas with mesh size ξ between 200 and 500 nm as schematically sketched in Fig. 11. This is in fair agreement with the average mesh size $\xi_{MPT} = (180 \pm 50)$ nm calculated from the MSD traces of the 510 nm particles with slope close to zero (see Table 2 next session).

3.2.4. Heterogeneity length scale of Carbopol solutions

A direct visualization of the solution microstructure can be obtained by a Delaunay triangulation of the focal plane images using the average positions of the tracer particles as generators. Around each particle a so-called Voronoi cell is constructed including all points closer to that particle than to any other particle in the plane [52]. Fig. 12A–E shows Voronoi diagrams for Carbopol 0.1, 0.2, 0.3, 0.4 and 0.75% solutions, respectively. These representations allow for a direct mapping of the solutions microstructure in terms of viscous (white) and elastic (black) regions corresponding to dMSD/dτ > 0.5 and dMSD/dτ < 0.5, respectively. In other words, polymer concentration fluctuations in the solutions are imaged here for the first time based on a "rheological contrast". At low Carbopol concentration (0.1%), a majority of the solution is viscous with very few elastic inclusions. As the polymer concentration increases the total fraction of viscous areas decreases continuously, finally reaching a structure consisting of isolated individual viscous areas of about 5–10 μm in diameter separated from each other by ~10–20 μm at 0.75% polymer concentration. Fig. 12F shows the fraction of image area attributed to viscous regions as a function of Carbopol concentration. This quantity decreases from 85% to 21% when Carbopol concentration increases from 0.1% to 0.75% respectively. At the same time, the number of individual, disconnected viscous regions increases from 1 to 40.

Table 2 shows the variation of the apparent viscosity η_{app}, plateau modulus G_0 and mesh size ξ_{MPT} with Carbopol concentration as determined from MPT measurements. The quantity η_{app} corresponds to the apparent viscosity in the viscous regions and has been determined from MSD traces with slope >0.5 using the relation $\langle \Delta \vec{r}^2(\tau) \rangle = 4D\tau$ in combination with the Stokes–Einstein relation $D = k_B T/6\pi\eta a$ including the diffusion coefficient D and the tracer particle radius a. This latter equation holds for particles freely diffusing in an infinite medium. In our case viscous regions are surrounded by highly elastic areas. These boundaries modify the hydrodynamics of the diffusing particles and essentially lead to a

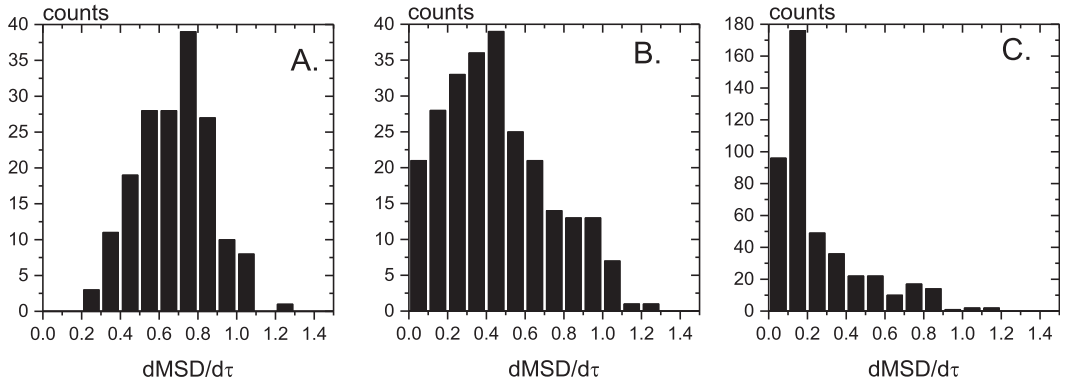

Fig. 9. Distribution of MSD slopes measured at time lag of 3s for microspheres (500 nm) dispersed in aqueous solutions of Carbopol 0.1% (A), 0.3% (B) and 0.75% (C).

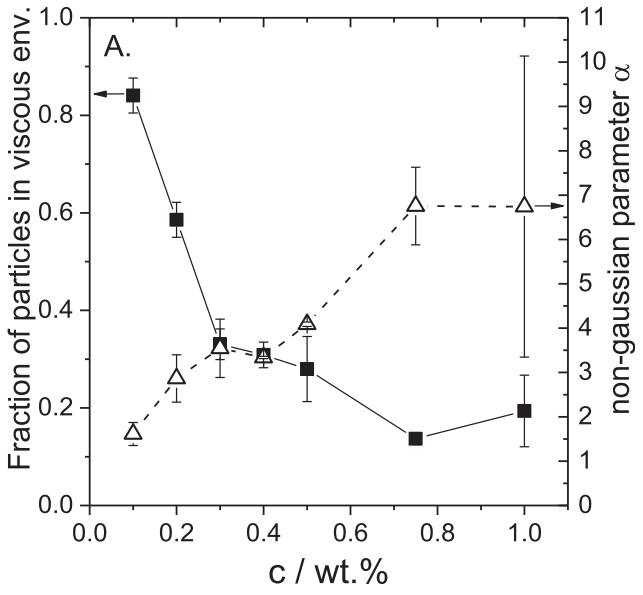

Fig. 10. Fraction of particles in a viscous environment (squares) and non-gaussian parameter α (triangles) as a function of Carbopol concentration.

decrease of the diffusion coefficient as it has been discussed in the literature extensively [53–56]. Accordingly calculated viscosity is higher than the true viscosity of the surrounding liquid and thus is termed apparent viscosity η_{app} in the following. The storage modulus G_0 has been determined from MSD traces with slope close to zero, i.e. from particles moving in a predominantly elastic environment using the relation $G_{0,app} = \frac{2k_BT}{3\pi a\langle \Delta \vec{r}^{\,2}(\tau)\rangle}$. The apparent mesh size is then obtained from $G_{0,app} = \frac{k_BT}{\xi^3_{MPT}}$ according to the classical rubber elasticity.

We observe a continuous increase of η_{app} in the viscous regions from 45 to 148 mPa as Carbopol concentration increases from 0.1 to 0.75%. This increase is supposed to be due to an increase of polymer concentration within the viscous regions, but it has to be kept in mind that these viscous regions shrink in size (see Fig. 12 A–E) and hence the measured diffusion coefficient of the tracer particles may decrease due to the above mentioned confinement effects. The Brownian motion of particles in the vicinity of a wall has been studied, both theoretically [53] and experimentally [54,55]. Lançon et al. [56] have shown that the diffusion coefficient of spherical colloidal particles between parallel walls strongly decreases when the channel width approaches the particle diameter. They report a 30% reduction of the diffusion coefficient perpendicular to the wall for a confinement ratio of 10, i.e. when the distance between the walls is 10 times the particle diameter and a 50% reduction for a confinement ratio of 5. This might serve as a reasonable estimate of the confinement effect here and would correspond to an increase of apparent viscosity by a factor of 1.33–2, which is not so far from what is observed when Carbopol concentration is increased from 0.1 % to 0.75 % and may account at least partly for the observed increase in η_{app}.

Table 2
apparent viscosity η_{app}, plateau modulus G_0 and mesh size ξ_{MPT} as determined from MPT measurements for Carbopol solutions of different viscosity.

Conc./wt%	η_{app}/mPas	$G_{0,app}$/Pa	ξ_{MPT}/nm
0.1	45 ± 16	0.27 ± 0.2	281 ± 101
0.2	46 ± 23	0.59 ± 0.5	231 ± 82
0.3	66 ± 27	1.06 ± 0.8	179 ± 49
0.4	89 ± 37	1.85 ± 1.6	160 ± 59
0.75	148 ± 85	8.5 ± 2.0	78 ± 36

The plateau modulus $G_{0,app}$ in the elastic regions increases from 0.27 to 8.5 Pa in the above mentioned concentration range indicating an increasing crosslink density. The corresponding mesh size ξ decreases from 281 to 78 nm. These values are much higher than those obtained from bulk measurements, i.e. for Carbopol 0.3%, $\xi_{Bulk} = 55\ nm < \xi_{MPT} = 179\ nm$, and this discrepancy is attributed to the inhomogeneity of the material. The ξ_{MPT} values are much smaller than the diameter of the tracer particles and characterize the elastic properties and network structure in the vicinity of the corresponding tracer particles. Based on light scattering data [51] and our MPT results especially the Voronoi diagrams we can describe the microstructure of Carbopol solutions in different concentration regimes. At low concentration individual microgel particles consisting of a highly cross-linked core regions surrounded by an expended shell roughly 20 μm in diameter are present in the solution. The cross-link or entanglement density in this shell is so low that the tracer particles can diffuse freely, only a small fraction of tracers is elastically trapped presumably in regions where microgel particles interpenetrate and the mesh size if the polymer network decreases well below 500 nm (see Fig. 12A).

When increasing the polymer concentration, overlap among microgel particles increases and corresponding elastic regions form an interconnected sample-spanning network. At 0.2% polymer concentration both the elastic regions as well as the viscous regions are connected among themselves throughout the sample (see Fig. 12B). But at higher polymer concentration the viscous regions are isolated and shrink more and more in size as shown in Fig. 12C–E.

4. Conclusions

MPT in combination with classical bulk mechanical rheometry has been used to characterize the structural and viscoelastic microheterogeneity of three commercial acrylic thickeners in

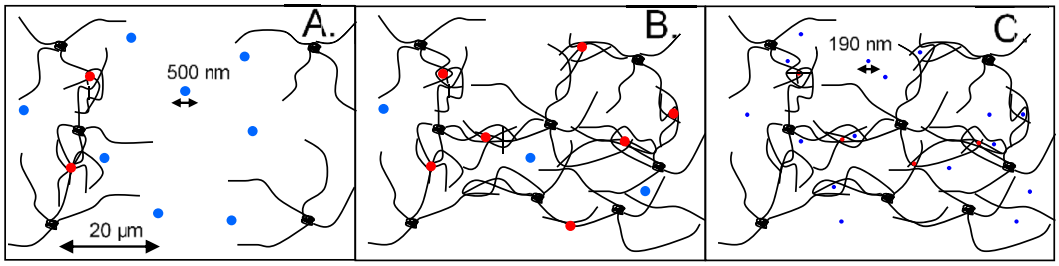

Fig. 11. Illustrations representing the microstructure of Carbopol at concentrations of 0.1% (A) and 0.3% (B) with tracer particles of diameter 510 nm, 0.3% with tracer particles of diameter 190 nm (C). Black dots represent the highly crosslinked cores of the microgels, the wiggly lines the surrounding shell. Blue dots represent tracer particles in a viscous environment and red ones particles trapped in elastic regions. The number of particles corresponds to the relative values given in Fig. 10.

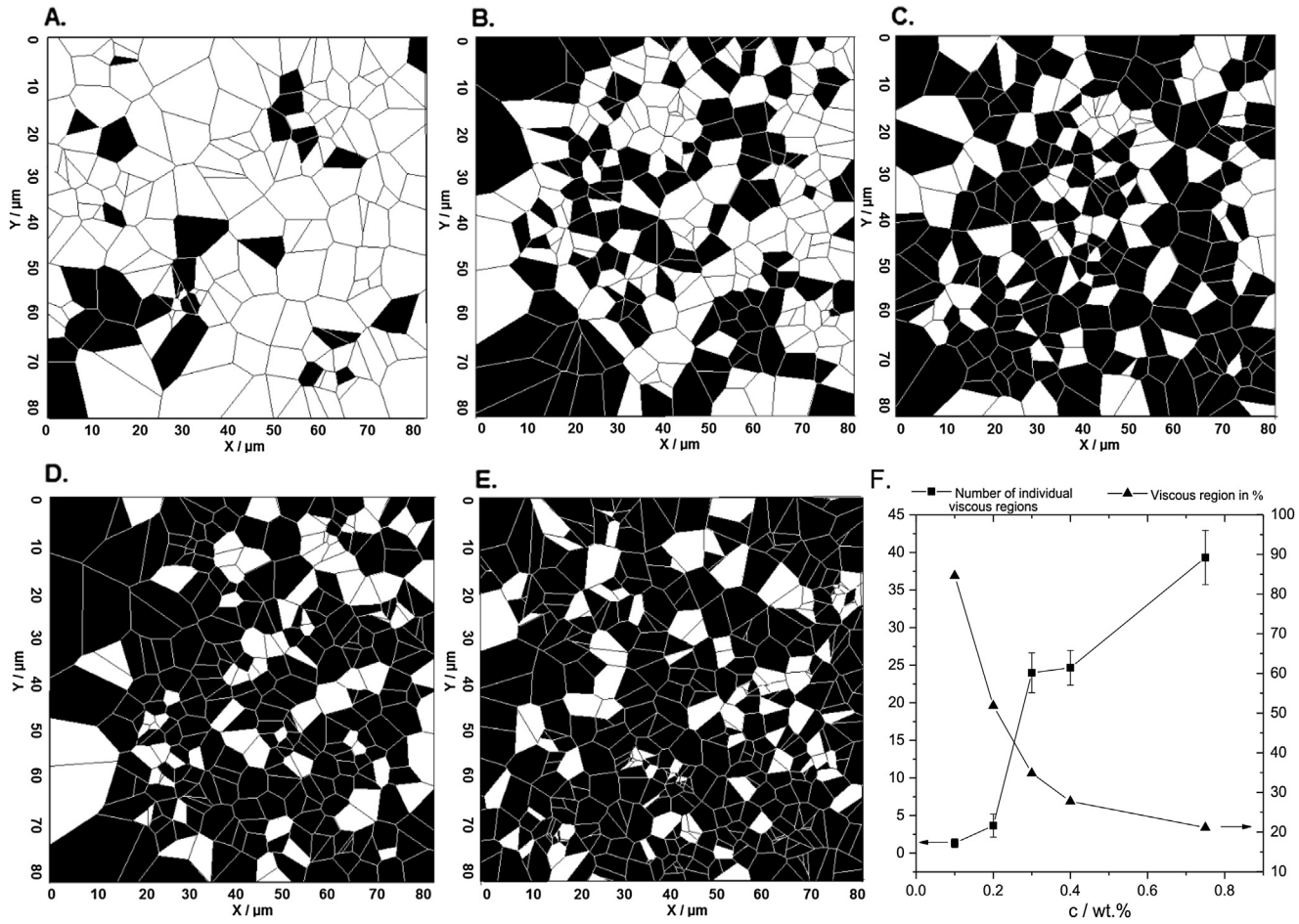

Fig. 12. Voronoi diagrams for Carbopol 0.1% (A), 0.2% (B), 0.3% (C), 0.4% (D) and 0.75% (E) based on experiments with 510 nm tracer particles. Viscous areas are in white and elastic areas in black. Number of individual viscous region (square) and viscous region in % (triangle) as a function of Carbopol concentration (F).

aqueous solutions at technically relevant polymer concentrations. From bulk rheology we found for Carbopol solutions a higher elasticity at low polymer concentration and a weaker dependence of the storage modulus on concentration than for the Sterocoll and Viscalex solutions. MPT experiments confirm that these two latter systems form pre-dominantly elastic polymeric network with a mesh size <200 nm in the concentration range investigated here. In contrast, Carbopol solutions are highly heterogeneous on a micrometer length scale and the degree of heterogeneity as characterized by the non-Gaussian parameter α obtained from a van-Hove analysis of MPT data strongly increases with increasing polymer concentration. Predominately elastic and viscous regions within the solution can be identified based on the slope of the mean squared displacement (MSD) of the individual particle trajectories. This heterogeneity is directly imaged here for the first time using Voronoi diagrams. Carbopol solutions consist of microgel particles with a highly crosslinked core (500 nm in diameter) and a dilute shell (20 µm in diameter) with a mesh size larger than the tracer particles used in our MPT experiments. Elastic regions are formed when microgel particles overlap to reduce the mesh size of the polymer network below the size of the probe particles (500 nm). At low Carbopol concentration the solutions are predominately viscous with few elastic inclusions typically 10 µm in size. At intermediate concentrations sample-spanning, connected elastic and the viscous regions interpenetrate. Finally, at high polymer concentration viscous inclusions are found within an elastic matrix and the size of these inclusions decreases with increasing polymer concentration with a characteristic length scale of about 500 nm at 0.75% Carbopol concentration. Variation of the probe size reveals that the elastic regions themselves are heterogeneous including areas with mesh size <200 nm and a larger fraction with mesh size between 200 nm and 500 nm. The bulk modulus G^* of such heterogeneous systems depends on the specific properties of the predominantly elastic and viscous regions as well as the characteristic length scale of the corresponding concentration fluctuations. Development of an appropriate model for calculation of the bulk modulus $G^*(\omega)$ based on the micro-structural and micro-rheological data obtained from MPT experiments will be targeted in future research. This is of high technical relevance since the bulk modulus is tightly related to the thickening and application properties of such polymers and a correlation between microstructure, microrheology and bulk rheology is the key to a rational goal-oriented product design.

Acknowledgments

The authors thank BASF-SE (Ludwigshafen, Germany) and Lubrizol Advanced Materials (Cleveland, USA) for providing the three acrylic thickeners.

Appendix A. Supplementary data

Supplementary data related to this article can be found at http://dx.doi.org/10.1016/j.polymer.2014.12.041.

References

[1] Oppong FK, de Bruyn JR. Diffusion of microscopic tracer particles in a yield-stress fluid. J Newt Fluid Mech 2007;142:104–11.
[2] Oppong FK, et al. Microrheology and structure of a yield-stress polymer gel. Phys Rev E 2006;73:041405.
[3] Oppong FK, Bruyn JR. Mircorheology and jamming in a yield-stress fluid. Rheol Acta 2011;50(4):317–26.
[4] Oelschlaeger C, Willenbacher N, Neser S. Multiple-particle tracking (MPT) measurements of heterogeneities in acrylic thickener solutions. Progr Colloid Polym Sci 2008.
[5] Wang C, Tam KC, Tan CB. Dissolution and swelling behaviors of random and cross-linked methacrylic acid-ethyl acrylate copolymers. Langmuir 2005;21:4191–9.
[6] Ng WK, Tam KC, Jenkins RD. Rheological properties of methacrylic acid/ethyl acrylate co-polymer: comparison between an unmodified and hydrophobically modified system. Polymer 2001;42:249–59.
[7] Kheirandish S, et al. Shear and elongational flow behavior of acrylic thickener solutions. Part II: effect of gel content. Rheol Acta 2009;48:397–407.
[8] English RJ, et al. Associative polymers bearing n-alkyl hydrophobes: rheological evidence for microgel-like behavior. J Rheol 1999;43:1175–94.
[9] Apgar J, et al. Multiple-particle tracking measurements of heterogeneities in solutions of actin filaments and actin bundles. Biophys J 2000;79:1095–106.
[10] Ma L, et al. A 'hot-spot' mutation alters the mechanical properties of keratin filament networks. Nat Cell Biol 2001;3:503–6.
[11] Tseng Y. Microheterogeneity controls the rate of gelation of actin filament networks. J Biol Chem 2002a;277(20):18143–50.
[12] Tseng Y, Wirtz D. Mechanics and multiple-particle tracking microheterogeneity of a-actinin-cross-linked actin filament networks. Biophys J 2001;81:1643–56.
[13] Valentine MT, et al. Investigating the microenvironments of inhomogeneous soft materials with multiple particle tracking. Phys Rev E 2001;64:061506.
[14] Tseng Y, et al. How actin crosslinking and bundling proteins cooperate to generate an enhanced cell mechanical response. Biochem Biophys Res Commun 2005;334:183–92.
[15] Tseng Y, Kole PT, Wirtz D. Micromechanical mapping of live cells by multiple-particle-tracking microrheology. Biophys J 2002;83(20):3162–76.
[16] Tseng Y, et al. Local dynamics and viscoelastic properties of cell biological systems. Curr Opin Colloid Interface Sci 2002b;7:210–7.
[17] Heidemann SR, Wirtz D. Towards a regional approach to cell mechanics. Trends Cell Biol 2004;14(4):160–6.
[18] Lee JSH, et al. Ballistic intracellular nanorheology reveals ROCKhard cytoplasmic stiffening response to fluid flow. J Cell Sci 2006;119:1761–8.
[19] Kole TP, et al. Intracellular mechanics of migrating fibroblasts. Mol Biol Cell 2005;16:328–38.
[20] Dawson M, Wirtz D, Hanes. Enhanced viscoelasticity of human cystic fibrotic sputum correlates with increasing microheterogeneity in particle transport. J Biol Chem 2003;278(50):50393–401.
[21] Xu J, et al. Microheterogeneity and microrheology of wheat gliadin suspensions studied by multiple-particle tracking. Biomacromolecules 2002;3:92–9.
[22] Goodman A, Tseng Y, Wirtz D. Effect of length, topology, and concentration on the microviscosity and microheterogeneity of DNA solutions. J Mol Biol 2002;323:199–215.
[23] Panorchan P, Wirtz D, Tseng Y. Structure-function relationship of biological gels revealed by multiple-particle tracking and differential interference contrast microscopy: the case of human lamin networks. Phys Rev E 2004;70:041906.
[24] Caggioni M, et al. Rheology and microrheology of a microstructured fluid: the gellan gum case. J Rheol 2007;51(5):851–65.
[25] Wirtz D. Particle-tracking microrheology of living cells: principles and applications. Annu Rev Fluid Mech 2009;38:301–26.
[26] Squires TM, Mason TG. Fluid mechanics of microrheology. Annu Rev Fluid Mech 2010;42:413–38.
[27] Mason TG, Weitz D. Optical measurements of frequency-dependent linear viscoelastic moduli of complex fluids. Phys Rev Lett 1995;74:1250–3.
[28] Tseng Y, Kole T, Wirtz D. Micromechnical mapping of live cells by multiple-particle-tracking microrheology. Biophys J 2002b;83:3162–76.
[29] Tolić-Nørrelykke I, et al. Anomalous diffusion in living yeast cells. Phys Rev Lett 2004;93(7).
[30] Rahman A. Correlations in the motion of atoms in liquid argon. Phys Rev 1964;136(2A):A405–11.
[31] Weeks ER. Three-dimensional direct imaging of structural relaxation near the colloidal glass transition. Science 2000;287(5453):627–31.
[32] Kegel WK, van Blaaderen A. Direct observation of dynamical heterogeneities in colloidal hard-sphere suspensions. Science 2000;287(5451):290–3.
[33] Van Hove L. Correlations in space and time and born approximation scattering in systems of interacting particles. Phys Rev 1954;95(1):249–62.
[34] Hansen JP, McDonald IR. In: Theory of the simple liquids. L. Academic Press; 1986.
[35] Baudonnet L, Grossiord J-L, Rodriquez F. Effect of dispersion stirring speed on the particle size distribution and rheological properties of three carbomers. J Dispers Sci Technol 2004;25(2):183–92.
[36] BASF technical data sheet for Sterocoll D (http://www.packaging.basf.com).
[37] BASF technical data sheet for Viscalex HV 30 (http://www.packaging.basf.com).
[38] Willenbacher N, Frechen T, Schuch H, Lettmann B. Waterborne automative coatings: application, particle interaction and microstructure. Eur Coatings J 1997;9:810–7.
[39] Dai S, Tam KC, Jenkins RD. Aggregation behavior of methacrylic acid/ethyl acrylate copolymer in dilute solutions. Eur Polym J 2000;36(12):2671–7.
[40] Technical report Noveon polymers technical bulletins. Noveon Pharmaceuticals; 2002.
[41] Lubrizol technical data sheet for Carbopol ETD 2050 (http://www.lubrizol.com).
[42] Kowalczyk A, Oelschlaeger C, Willenbacher N. Tracking errors in 2D multiple particle tracking microrheology, accepted November 2014 in Measurement Science and Technology.
[43] Crocker JC, Grier DG. Methods of digital video microscopy for solloidal studies. J Colloid Interface Sci 1996;179:298–310.
[44] Roberts GP, Barnes MS. New measurements of flow-curves for carbopol dispersions without slip artefacts. Rheol Acta 2001;40(499).
[45] Curran SJ, et al. Properties of carbopol solutions as models for yield-stress fluids. J food Sci 2002;67(1).
[46] Kim J-Y, et al. Rheological properties and microstructures of carbopol gel network system. Colloid Polym Sci 2003;281(7):614–23.
[47] Martinie L, Buggisch H, Willenbacher N. Apparent elongational yield stress of soft matter. J Rheol 2013;57(2):627–46.
[48] Kowalczyk A, Hochstein B, Stahle P, Willenbacher N. Characterization of complex fluids at very low frequency: experimental verification of the strain rate-frequency superposition (SRFS) method. Appl Rheol 2010;20(5):1–12.
[49] Rubinstein Michael, Colby RH. Polym Phys 2003.
[50] Savin T, Doyle PS. Static and dynamic errors in particle tracking microrheology. Biophys J 2005;88:623–38.
[51] Lee D, Gutowski IA, Bailey AE, Rubatat L, de Bruyn JR, Frisken BJ. Phys Rev E 2011;83:031401.
[52] Okabe A, Boots B, Sugihara K, Chiu SN. Spatial tessellations – concepts and applications of voronoi diagrams. 2nd ed. John Wiley; 2000.
[53] Happel J, Brenner H. Low Reynolds number hydrodynamics. Martinus Nijhoff Publishers; 1983.
[54] Feitosa MIM, Mesquita ON. Wall-drag effect on diffusion of colloidal particles near surfaces: a photon correlation study. Phys Rev A 1991;44(10):6677–85.
[55] Faucheux LP, Libchaber AJ. Confined brownian motion. Phys Rev E 1994;49(6):5158–63.
[56] Lançon P, Batrouni G, Lobry L, Ostrowsky N. Brownian walker in a confined geometry leading to a space-dependent diffusion coefficient. Phys A 2002;304(1–2):65–76.